Equilibrium Analysis of Tokamak Plasma Including the Eddy Current Effects in TOKASTAR-2*)

Ryohei IKEDA, Takaaki FUJITA, Hideki ARIMOTO, Atsushi OKAMOTO, Kouhei YASUDA, Sora KIMATA and Keitaro KADO

Graduate School of Engineering, Nagoya University, Furo-cho, Chikusa-ku, Nagoya 464-8603, Japan

(Received 6 January 2020 / Accepted 22 May 2020)

The equilibrium analysis including the eddy current effect was performed for TOKASTAR-2 tokamak plasma by using TOSCA code that treated the vacuum vessel as the 2D axisymmetric model. In measurement of the vacuum magnetic field without plasma, it was found that the measured magnetic field and the calculated one using the model configuration which was based on the TOKASTAR-2 design did not agree. To improve the model, some parameters in the model (e.g. coil positions) were adjusted to minimize the difference between the calculated field and the measured one. In the equilibrium analysis, the poloidal beta β_P and the plasma internal inductance l_i were determined minimizing the difference between the calculated field and the measured one for external probes. It was found that the solution calculated by the external measurement was roughly consistent with the internal field measurement, with difference in the plasma internal inductance of 0.10. The high-speed camera and the internal measurement results indicated that the shape and position of the plasma also have small errors. More improvement in the wall model would be needed to resolve these discrepancies.

Keywords: TOKASTAR-2, tokamak plasma, eddy current, MHD equilibrium analysis

DOI: 10.1585/pfr.15.2402047

1. Introduction

The TOKASTAR-2 device is able to generate tokamak and helical magnetic field configurations independently [1–3]. This device is a low aspect ratio ($A < 3$) one and a typical plasma major radius is ~0.11 m. One of the main purposes of TOKASTAR-2 is the verification of the stabilization of the tokamak plasma position by helical field [4].

Figure 1 shows a schematic view of TOKASTAR-2. This device has both the tokamak coil system and the stellarator coil system. The tokamak coil system consists of three-blocks Ohmic Heating (OH) coils, a pair of Pulsed Vertical Field (PVF) coils, a pair of Shape Control (SC) coils and eight Toroidal Field (TF) coils. In the tokamak operation, The OH coils, the PVF coils, the SC coils, and the TF coils are connected to pulsed power supplies with capacity banks. The toroidal field strength is ~0.1 T and pre-discharge is generated with electron cyclotron resonance heating (ECRH) by a microwave of 2.45 GHz. The OH coils induce a plasma current (~2.2 kA, ~0.5 ms) and the PVF coils and the SC coils form the equilibrium field.

Stabilization of the tokamak plasma position by applying the helical field is owing to the Lorenz force generated by the effective poloidal field of the helical field on the plasma current. In TOKASTAR-2, stabilization of the radial plasma position by helical field was observed by

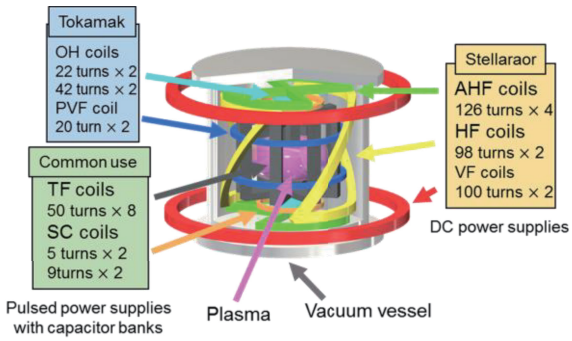

Fig. 1 Schematic view of TOKASTAR-2.

three methods. The first one is the internal magnetic field measurement using a movable magnetic probe array [5,6]. The current density profile can be obtained as well as the plasma radial position by this method. However, the vertical position of the plasma cannot be obtained. Furthermore, inserting the magnetic probe into the plasma affects the plasma position and the plasma current largely. From these reasons, this method is not suitable for study of position stabilization by the helical field. The second one is a high-speed camera [7]. This method does not affect the plasma at all. However, because of the integration of light along the sight line and the light reflections inside the vacuum vessel, it is difficult to determine the boundary of the plasma clearly. The third one is the Filament Current Approximation (FCA) method with external magnetic

author's e-mail: fujita@energy.nagoya-u.ac.jp

*) This article is based on the presentation at the 28th International Toki Conference on Plasma and Fusion Research (ITC28).

measurement [8]. In the FCA method the plasma current is modeled by six ring filaments and the plasma position is determined by using the signals of the magnetic probes and the magnetic flux loops. In the FCA method, $\beta_P + l_i/2$ can be evaluated from the line integral of magnetic field [9], where β_P is the poloidal beta and l_i is the plasma internal inductance. From this it would be possible to evaluate l_i, which characterizes the plasma current density profile, since β_P is small in TOKASTAR-2 as shown in section 4.1. The evaluation of $\beta_P + l_i/2$ is, however, not available at present in the FCA method used in TOKASTAR-2. Since the plasma current density profile is not obtained in the FCA method, it is not possible to calculate the Lorenz force and evaluate the stabilization effect quantitatively. So, we needed a new method for determining the plasma position and the current density profile without influence on the plasma.

In this paper, by solving the magnetohydrodynamics (MHD) equilibrium equation, we evaluated the plasma current density profiles with external magnetic measurements. By finding MHD equilibrium consistent with external magnetic measurements, it is possible to evaluate $\beta_P + l_i/2$, and also β_P and l_i separately for noncircular plasmas [10]. Since the eddy current is driven largely in the TOKASTAR-2 vacuum vessel, the magnetic field by the eddy current needs to be precisely evaluated and be considered in the MHD equilibrium analysis. In this article, we report the results of the equilibrium analysis including eddy current effect using the experiment data in TOKASATAR-2 for the first time and discuss the validity of the solution. As the first step of the verification, we inserted the probe to the tokamak plasma and compared the equilibrium solution and the experimental measurement.

2. Measuring Method

Figure 2 (a) shows a layout of the magnetic sensors in TOKASTAR-2. Three types of sensors are installed.

The first type is the magnetic probe array (MPA) [8]. It consists of 16 sensor coils which are installed in ceramic rods behind the poloidal limiter. It thus does not touch the plasma. The upper-side two coils (CH 4, 6) and the lower-side two coils (CH 12, 14) measure the radial field and the other 12 coils measures the vertical field.

The second type is the magnetic flux loop (FL). Four one-turn FLs are installed at $R = 0.06$ m, $Z = \pm 0.13$ m and $R = 0.18$ m, $Z = \pm 0.10$ m. They measure not only the poloidal magnetic flux but also the toroidal one-turn voltage. The MPA and the FLs are used in the FCA method.

The third type is the multi-channel magnetic probe (MMP) [6]. It contains nine sensor coils that measure the vertical field. The MMP is located on the equator plane and at the toroidal angle of one of the four large ports on the side wall of the vacuum vessel as shown in Fig. 2 (b). The MMP can be moved radially shot by shot and is inserted into plasma when the magnetic field inside the plasma is

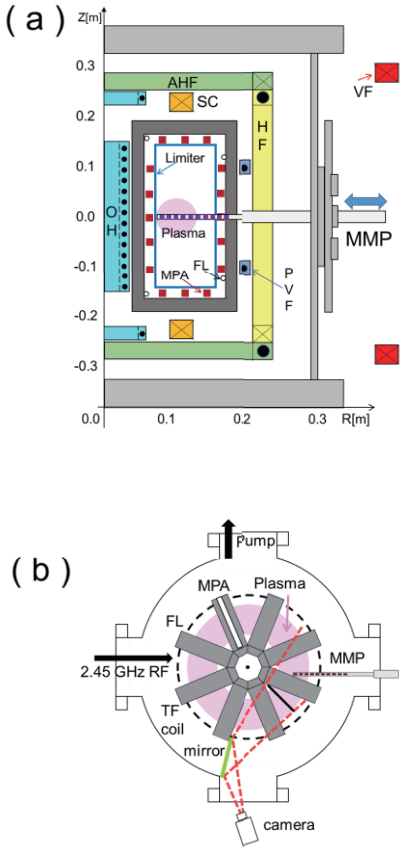

Fig. 2 (a) Cross-section view and (b) plane view of the TOKASTAR-2.

measured. It is pulled out behind the outer limiter when not used. The MMP is not used in the FCA method. In this study, the MMP is used for comparison with the equilibrium solutions with external field measurement to verify its accuracy.

The measured field B^{total} and the measured flux ψ^{total} consist of those by the coils (B^{coil} and ψ^{coil}), those by the plasma current (B^{plasma} and ψ^{plasma}) and those by the eddy current (B^{eddy} and ψ^{eddy}):

$$B^{total} = B^{coil} + B^{plasma} + B^{eddy}, \quad (1)$$

$$\psi^{total} = \psi^{coil} + \psi^{plasma} + \psi^{eddy}. \quad (2)$$

3. Analysis Method

We calculated the equilibrium of tokamak plasmas with the tokamak operation scenario circuit analysis (TOSCA) code. This code solves the equilibrium equation including the eddy current.

3.1 Analysis method of the eddy current

In TOSCA, the vacuum vessel is modeled by circular passive conductors with rectangular cross-section, while the Grad Shafranov equation is solved in rectangular grid to obtain MHD equilibrium. The eddy current distribution is obtained by solving 2D axisymmetric circuit equations. The circuit equation for the ith conductor is written as

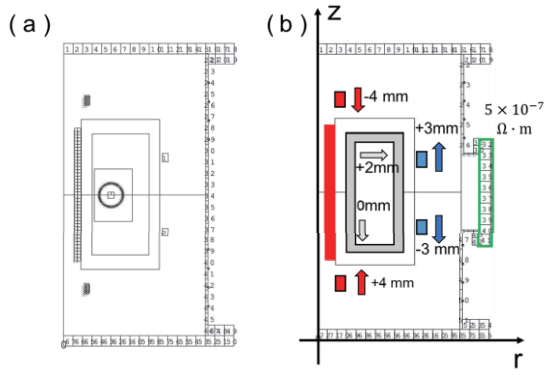

Fig. 3 (a) The original model and (b) the new model of TOKASTAR-2.

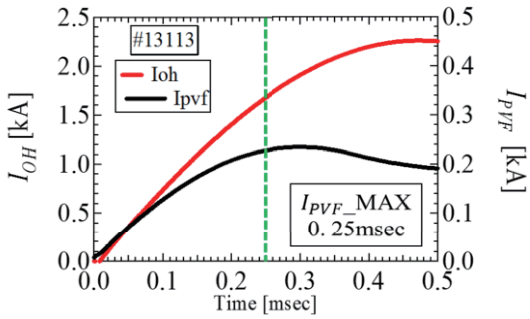

Fig. 4 The time evolution of the coil current. We calculated the error at 0.25 ms when the PVF coil current became maximum.

$$R_i I_i + \sum_{j=1}^{n_{cw}} M_{i,j}\frac{dI_j}{dt} + \sum_{l=1}^{n_{coil}} \widehat{M}_{i,l}\frac{d\hat{I}_l}{dt} + \frac{d}{dt}(\overline{M}_i I_P) = 0, \tag{3}$$

where n_{cw} and n_{coil} are the total numbers of conductors and magnetic coils, I_j, $\hat{I}_l$ and I_P are the jth eddy current, the lth coil current and the plasma current, R_i is the resistance of ith conductor and $M_{i,j}$, $\widehat{M}_{i,l}$ and $\overline{M}_i$ are the mutual inductance between the ith conductor and the jth conductor, the lth coil and the plasma current, respectively.

Figure 3 (a) shows the original wall model which was based on the TOKASTAR-2 design. In this model the coils are located at the positions in the design and four large ports on the side wall shown in Fig. 2 (b) are neglected.

The vacuum magnetic field ($B^{coil} + B^{eddy}$) was measured by MPA in a shot turning on the circuits for the OH coil and the PVF coil without plasma, where B^{plasma} and ψ^{plasma} were zero in eqs. (1) and (2), and was compared with the TOSCA calculation. Figure 4 shows time evolution of the OH coil current and the PVF coil current. The charging voltages of capacitor banks were the nearly same as those in the plasma experiment described in section 4; $V_{OH} = 2.0$ kV and $V_{PVF} = 0.30$ kV. Comparison was made at $t = 0.25$ ms when the PVF coil current I_{PVF} was close to the maximum. Figure 5 shows the difference between the measurement and the calculation. In Fig. 5 (b), the blue

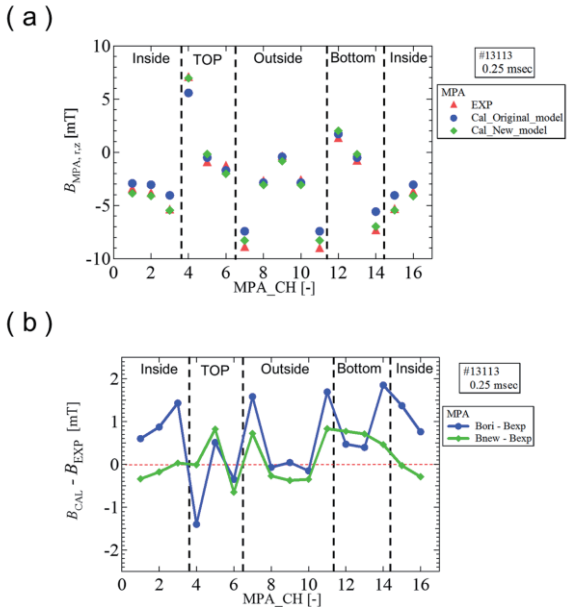

Fig. 5 (a) Comparison and (b) difference between the measured vacuum magnetic fields (red triangles) and the calculated vacuum magnetic fields with TOSCA (blue circles and green diamonds) at 0.25 ms. The blue circles and the green diamonds denote the values obtained by using the original model and the new model, respectively.

Table 1 Scanned range of parameters. The center block of the OH coil is fixed as a reference position of the other coils and the sensors.

Targets	Parameters	Range
MPA position	r, z	−5 ~ +5 [mm]
PVF and OH Coil Position	z	−5 ~ +5 [mm]
Wall Resistivity	ρ	5~10 [$\times 10^{-7}\Omega$m]

circular symbols denote the difference between the calculation using the original model and the experiment one, $B_{ori,CAL} - B_{Exp}$. Large difference is found in some channels. We considered two possible causes; the one is the installation errors of the coils and the magnetic probes and the other is the complicated 3D shape of the vacuum vessel, both of which are not considered in the original model.

To include the effect of the four large side ports of the vessel, we added side ports to the vessel model and scanned its resistivity. To include the effect of installation errors of the coils and the magnetic probes, we scanned the positions of the coils and the magnetic probe. The ranges of scan is shown in Table 1. Here the resistivity was 7.2×10^{-7} Ω·m, the value of the stainless steel, in the other parts of the vessel. The optimum values of the scanned parameters were determined to minimize the error E_{model} between the measured values and the calculated values defined by

$$E_{\mathrm{model}}(t) = \sum_{i=1}^{16} \left(B_{\mathrm{MPA},i}^{\mathrm{tot,cal}} - B_{\mathrm{MPA},i}^{\mathrm{tot,exp}} \right)^2, \quad (4)$$

where t is the error calculation time, 0.25 ms. The determined values are shown in Fig. 3 (b). The difference between the magnetic field calculated by the new model and the experimental one, $B_{\mathrm{new,CAL}} - B_{\mathrm{Exp}}$, is shown by green diamond symbols in Fig. 5 (b). The difference is totally smaller than that calculated by the old model, though non-negligible differences remain. The improvement was also found at other times around 0.25 ms (e.g. 0.2 and 0.3 ms), while the difference was larger at later times. The new model was used in the equilibrium analysis of tokamak plasma including the eddy current effect presented in section 4.

3.2 Method of equilibrium analysis

In TOSCA, the free-boundary Grad Shafranov equation is solved by the Buneman Poisson solver. The target shape of the last closed flux surface, LCFS is determined by the plasma major radius R_{P}, the height of the plasma center Z_{P}, the plasma minor radius a_{P}, the elongation κ and the triangularity δ. The currents of some poloidal field coils, called free coils, are determined to adjust the shape of LCFS to the target while the current of other coils, called fixed coils, are fixed. In this study, the radial profiles of the current density j_{P} are given by:

$$j_{\mathrm{P}}(\tilde{\psi}, R) = j_0 \left\{ \beta_{\mathrm{J}} \frac{R}{R_{\mathrm{P}}} + (1-\beta_{\mathrm{J}}) \frac{R_{\mathrm{P}}}{R} \right\} \times \left\{ (1-(1-\tilde{\psi})^{C_{\mathrm{n}}})^{C_{\mathrm{m}}} \left(1 - \alpha_{\mathrm{d}} \left(\frac{\tilde{\psi} - \alpha_{\mathrm{c}}}{1-\alpha_{\mathrm{c}}} \right)^2 \right) \right\}, \quad (5)$$

$$\tilde{\psi} \equiv \frac{\psi - \psi_{\mathrm{SURF}}}{\psi_{\mathrm{AXIS}} - \psi_{\mathrm{SURF}}}, \quad (6)$$

where C_{n} is generally set to 1, parameters j_0, β_{J} and C_{m} are determined to have $I_{\mathrm{P}}, \beta_{\mathrm{J}}$ and l_{i} equal to given values α_{c} and α_{d} which are related to the radial position and the depth of the hollow current are set to 0.2 and 0.7, respectively. If α_{d} is 0, the current profiles are limited to broad or center peak with $l_{\mathrm{i}} \geq 0.5$. In this paper, the above values are used to have profiles with $l_{\mathrm{i}} < 0.5$. In eq. (6), ψ_{SURF} and ψ_{AXIS} are the poloidal flux at the plasma surface and the magnetic axis so that $\tilde{\psi}$ is 0 at the magnetic surface and 1 at the magnetic axis. The eddy current calculation is inserted between the times of equilibrium calculations. Then, the self-consistent equilibrium solution including the effect of the eddy currents is determined. The circuit equation for the eddy current is a differential equation, which means that the results strongly depends on the initial condition, then we should pay attention the initial time to start the calculation. In this study, input parameters are given as shown in Table 2. The PVF coil is regarded as the free coil. β_{P} and l_{i} were assumed to be constant during the discharge.

As the plasma major radius R_{P}, the height of the plasma center Z_{P}, the plasma minor radius a_{P} and the elongation, those of the last flux surface calculated by the FCA method was used at each time step. Since the triangularity δ was usually approximately 0 in the past FCA analysis, the input value to TOSCA was also set to 0. In the FCA method used in this study, the eddy current was analyzed by the same way as the TOSCA calculation using the 2D conducting wall model, while the measured vacuum field was used in [8]. The eddy current calculated by the FCA method and the one calculated by TOSCA were consistent, when the free coil current was close to the experiment value. The initial time to start the equilibrium analysis was set to the time when the accuracy of the FCA analysis was enough high.

Table 2 TOSCA input parameters. We assume that l_{i} and β_{P} are constants at all time.

Input Parameters	Conditions
I_{P} and I_{OH}	Experimental measurements
Coil and vacuum vessel blocks	The optimal model (Fig.3 (b))
plasma geometric parameters (a_{P}, R_{P}, Z_{p}, κ)	FCA results
plasma current parameter (l_{i}, β_{P})	any value ($l_{\mathrm{i}} \geq 0.4$)

The vacuum vertical field needed to maintain the radial force balance, B_{z}, is given by the equation below [11] for low beta circular plasmas

$$B_{\mathrm{z}} = -\frac{\mu_0 I_{\mathrm{P}}}{4\pi R_{\mathrm{P}}} \left[\ln \frac{8R_{\mathrm{P}}}{a_{\mathrm{P}}} + \beta_{\mathrm{P}} + \frac{l_{\mathrm{i}}}{2} - \frac{1}{2} \right], \quad (7)$$

where μ_0 is the vacuum permeability. The above equation suggests that the PVF coil current has a relationship with β_P and l_{i}. Then, the PVF coil current was adjusted to have an equilibrium with given parameter, including the shape of LCFS, in TOSCA. We find the equilibrium where the PVF coil current agrees with the experimental value.

3.3 Estimation of values of l_{i} and β_{P}

The β_{P} and l_{i} at $t = 2.733$ ms of the plasma shown in Fig. 6 are evaluated based on the electron temperature and the electron density measurement, and magnetic probe measurement inside plasmas for the similar discharge plasma.

The value of β_{P} can be estimated by the measurement of the electron temperature and the electron density. β_{P} is defined by

$$\beta_{\mathrm{P}} = \frac{\langle P \rangle}{\frac{B_{\mathrm{P}}^2(a)}{2\mu_0}} \approx \frac{e n_{\mathrm{e}} T_{\mathrm{e}}}{\frac{1}{2\mu_0}\left(\frac{\mu_0 I_{\mathrm{P}}}{2\pi a_{\mathrm{P}}}\right)^2} = \frac{2\pi a_{\mathrm{P}}^2 e n_{\mathrm{e}} T_{\mathrm{e}}}{I_{\mathrm{P}}^2} \times 10^7, \quad (8)$$

where e is elementary charge, $n_{\mathrm{e}}[\mathrm{m}^{-3}]$ is the electron density, T_{e} [eV] is the electron temperature and I_{P} [A] is the total plasma current. The ion temperature is assumed 0. In the previous study [12], $n_{\mathrm{e}} = 2.5 \times 10^{18}\,\mathrm{m}^{-3}$ and $T_{\mathrm{e}} = 10$ eV were estimated for helium plasma with $I_{\mathrm{P}} = 1.5$ kA by the spectroscopic measurement. This helium plasma was generated by the similar OH coil current waveform

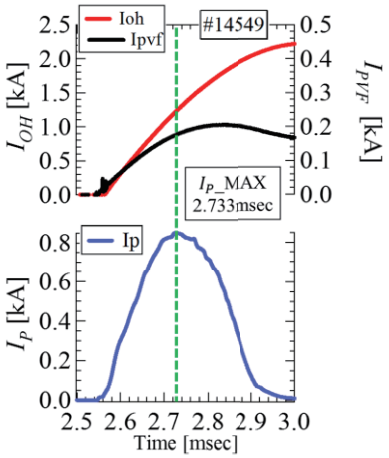

Fig. 6 The time evolution of (top) the coil currents and (bottom) the plasma current. The equilibrium analysis was done at 2.733 ms or when the plasma current became maximum, indicated by a vertical dotted line.

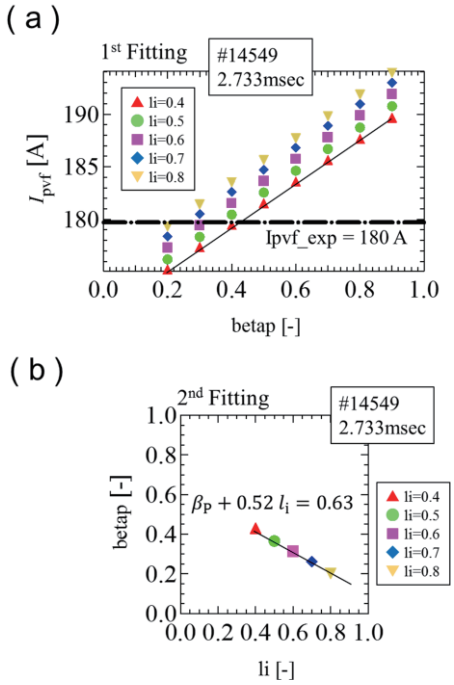

Fig. 7 (a) $I_{PVF,CAL}$ vs β_P for each l_i and an example of fitting for $l_i = 0.4$. (b) β_P vs l_i and the fitting line which satisfies $I_{PVF,CAL} = I_{PVF,EXP}$.

used in section 4, but no probes were inserted into plasma. For $a_P = 0.04$ m as the representative value, the value of β_P was calculated as about 0.2. If we consider the ion temperature, the value of β_P is larger. For example, assuming the ion temperature $T_i \approx T_e$ and the ion density $n_i \approx n_e$, the value of β_P become about 0.4 that is close to the value determined from the equilibrium analysis in section 4.

The value of l_i can be estimated by the measurement of the internal magnetic field. To estimate the value, we performed the same plasma discharge and measured the internal vertical field with the MMP inserted into the plasma in section 4. As a result of the measurement, it was found that the current density profile was nearly flat by using the method described [5, 6]. Hence the value of l_i is estimated about 0.5, which corresponds to the flat current density profile.

4. Results

Figure 6 shows the time evolution of the OH coil current, the PVF coil current and the plasma current in a shot used for the equilibrium analysis. We started the equilibrium calculation at $t = 2.632$ ms when the plasma current was 481 A. The initial conditions for the eddy current calculation were set to those calculated by FCA model at $t = 2.630$ ms. We calculated time evolution of equilibrium with intervals of typically 2 μs until $t = 2.733$ ms when the plasma current was maximum and the PVF coil current was 180 A. We focus on the results at $t = 2.733$ ms hereafter in this article. The charging voltages of capacitor banks for the PVF coil, the OH coil and the TF coil are $V_{PVF} = 0.28$ kV, $V_{OH} = 2.0$ kV, $V_{TF} = 1.1$ kV, respectively. The inductance of the TF coil is so large that the TF coil current is steady during the plasma current pulse. Nitrogen gas was used as working gas. The MMP was inserted through the plasma, up to its high-field-side edge, to measure the radial profile of the vertical magnetic field on the equator plane.

4.1 Results of equilibrium analysis

We find values of l_i and β_P which give an MHD equilibrium consistent with the PVF coil current and the external magnetic measurements. First, a relation between l_i and β_P to have the PVF coil current equal to the experimental value is determined and then a single set of l_i and β_P is selected to minimize errors between the calculated values and the experimental values of magnetic field at sensors of MPA.

A relation between l_i and β_P to have the PVF coil current equal to the experimental value is determined through the following three steps.

1. Both of l_i and β_P were roughly scanned and the PVF coil current $I_{PVF,CAL}$ was obtained for each case as shown by color symbols in Fig. 7 (a).
2. The $I_{PVF,CAL}$ was fitted by a linear function of β_P for each l_i, as shown by a black solid line in Fig. 7 (a), and the value of β_P satisfying the condition of $I_{PVF,CAL} = I_{PVF,EXP}$ was determined, as the intersection of the thin line and the thick dotted line in Fig. 7 (a).
3. Using the sets of (l_i, β_P) obtained in step 2, a relation between β_P and l_i was determined to have the PVF coil current equal to the experimental value (color symbols and the fitting line in Fig. 7 (b)).

Through the above three steps, a condition $\beta_P + 0.52 l_i =$

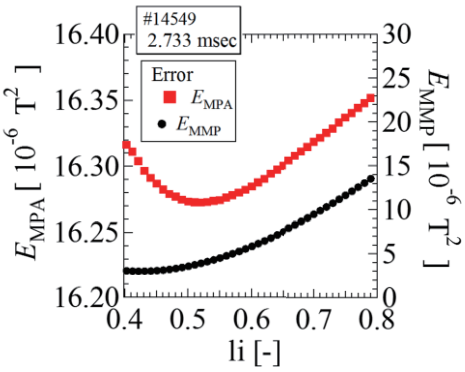

Fig. 8 The error between the measurement and the calculation by TOSCA at MPA positions (E_{MPA}, red line) at MMP positions (E_{MMP}, black line) as functions of l_i. The E_{MPA} is minimum at $l_i = 0.52$ while the E_{MMP} is minimum at $l_i = 0.42$.

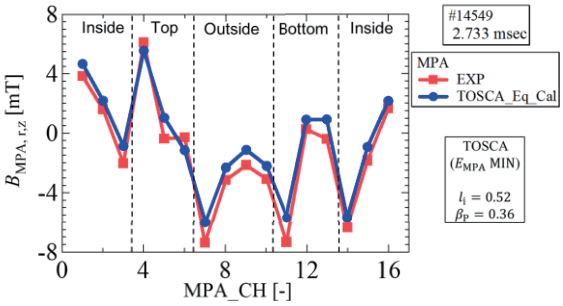

Fig. 9 The comparison between the measured total magnetic field (red line with squares) and the calculated total magnetic field by TOSCA (blue line with circles) at 2.733 ms.

0.63 for satisfying $I_{PVF,CAL} = I_{PVF,EXP}$ was obtained.

Next, to choose a set of (l_i, β_P) from this condition, we compared the magnetic field values. We scanned l_i from 0.4 to 0.8 with an interval of 0.01 on the line of $\beta_P + 0.52 l_i = 0.63$ and calculated the magnetic field at MPA positions in each (l_i, β_P). Then the error between E_{MPA} the measured values and the calculated values by TOSCA was calculated by

$$E_{MPA}(t) = \sum_{i=1}^{16} \left(B_{MPA,i}^{tot,CAL} - B_{MPA,i}^{tot,EXP} \right)^2 . \quad (9)$$

The optimum set of (l_i, β_P) was determined to minimize E_{MPA}. The dependence of E_{MPA} on l_i is shown by the red line in Fig. 8. $E_{MPA}(t)$ has its minimum at $l_i = 0.52$. As a result, the equilibrium with $l_i, \beta_P = (0.52, 0.36)$ was determined from the external measurement. Figure 9 shows the comparison of the magnetic field at the MPA positions. The calculated values by TOSCA were shifted toward the positive direction from the measured values by the MPA.

4.2 Comparison with the internal magnetic field measurement and camera image

In this section, validity of the equilibrium determined by external magnetic field measurement in section 4.1 is investigated by comparing it with the internal magnetic field measurement and the camera image.

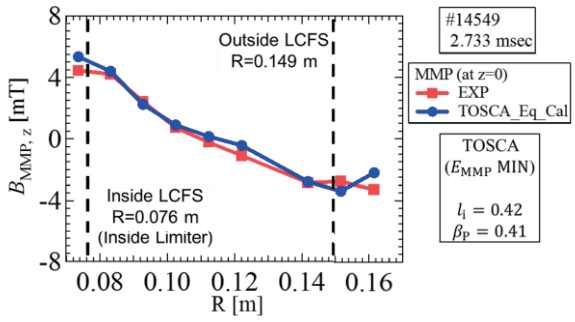

Fig. 10 Radial profiles of the measured total magnetic field (red line with squares) and the calculated total magnetic field (blue line with circles) at 2.733 ms.

Except using the MMP instead of the MPA, the method to obtain the equilibrium conditions is the same as used in section 4.1. We define an error on the MMP signals $E_{MMP}(t)$ by

$$E_{MMP}(t) = \sum_{i=1}^{9} \left(B_{MMP,i}^{tot,CAL} - B_{MMP,i}^{tot,EXP} \right)^2 . \quad (10)$$

The dependence of $E_{MMP}(t = 2.733\,\text{ms})$ on l_i is shown by the black line in Fig. 8. $E_{MMP}(t)$ has its minimum at $l_i = 0.42$. Namely, by using this error, the equilibrium with $(l_i, \beta_P) = (0.42, 0.41)$ was determined. The value of l_i is smaller by 0.10 than that obtained with the external measurement.

Figure 10 shows the measured magnetic field and the calculated magnetic field of the equilibrium solution on the equator plane. From this figure, it can be seen that the radial profiles of the magnetic field are nearly identical. However, the position of the outer plasma surface seems to be different. From the Ampere's low, the magnetic field outside the plasma, where there is no toroidal current, decreases in its magnitude as shown by the result of the equilibrium analysis in Fig. 10, where the outer plasma surface determined by TOSCA is located at $R = 0.149\,\text{m}$. On the other hand, the measured profile in Fig. 10 is nearly flat around that radius and seems to indicate that the outer plasma surface is located at a larger radius. That is, the area of the plasma was wider than that in the equilibrium analysis.

The position and the shape determined by external magnetic field measurement are compared with a high-speed camera image in Fig. 11. The area enclosed by the LCFS calculated by TOSCA almost overlaps with the plasma area shown by the camera. Although it was difficult to determine the plasma boundary using the camera image as mentioned in the introduction, the center position of the plasma could be determined roughly from the center of the emission intensity profile. Figure 12 shows the vertical distribution of the normalized emission intensity along

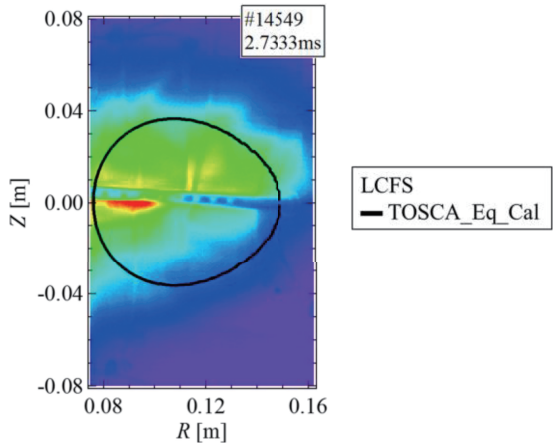

Fig. 11 A color image of the tokamak plasma measured the high-speed camera at 2.7333 ms and the last closed flux surface calculated by TOSCA at 2.733 ms.

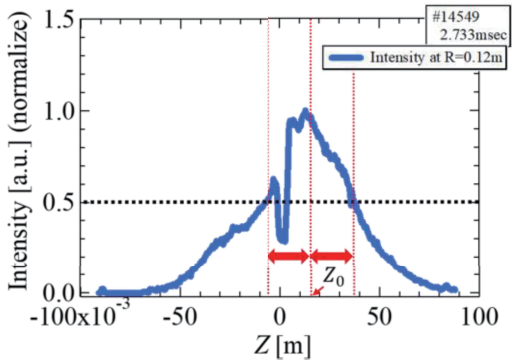

Fig. 12 The vertical distribution of the normalized emission intensity along $R = 0.12$ m at 2.733 msec.

$R = 0.12$ m at 2.733 msec. The R position of the plasma center was not obtained clearly, but the Z position could be obtained by the analysis of the intensity profile because the length of the sight line is vertically symmetric. The positions of the same intensity of 50% of the maximum intensity were $Z = -0.008$ m and $Z = 0.038$ m, and then the vertical position of the plasma center Z_0 was estimated to be about 0.015 m. On the other hand, the vertical position of the LCFS calculated by TOSCA was at the equatorial plane ($Z = 0$).

5. Discussion

The magnetic field error E_{MPA} was minimum with $(l_{\mathrm{i}}, \beta_{\mathrm{P}}) = (0.52, 0.36)$ and, on the other hand, the error was minimum with $(l_{\mathrm{i}}, \beta_{\mathrm{P}}) = (0.41, 0.41)$ as shown in Fig. 8. The difference in l_{i}, 0.10, is not so large and then the equilibrium determination with external measurement seems to be promising at least for rough estimation of the current density profile. This is somewhat surprising considering that the shape of the plasma is nearly circular and that the upper and lower magnetic probes are relatively apart from the plasma surface in particular with circular cross section. In fact, poor sensitivity of E_{MPA} on l_{i} is seen in Fig. 8. To confirm the validity of the equilibrium solution determined by the external measurement only, we need to compare the equilibrium solutions determined by the external measurements with the internal measurement for many shots with various discharge conditions.

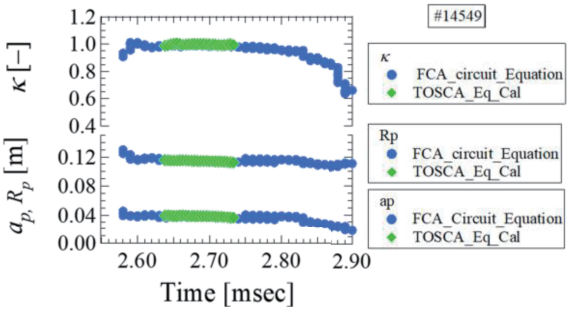

Fig. 13 The comparison of (top) the elongation and (bottom) the major and the minor radii calculated by the FCA used the circuit equation method (blue circles) and TOSCA (green diamonds).

Comparing the equilibrium solution with the internal magnetic field and the camera image, it was found that the center position and the area of the plasma seems to be different from the calculation from the equilibrium solution as shown in Fig. 10, Fig. 11 and Fig. 12. At present, we consider that one of the causes of this disagreement of the position and area seems to be the error in the vacuum field by the coil current and the eddy current that is calculated with the wall model of TOSCA, because the plasma shape was determined by the FCA method with eddy current calculation with the same wall model as TOSCA. Figure 13 shows κ, R_{P} and a_{P} calculated by the FCA using the circuit equation and TOSCA. Certainly, these values are consistent. Though we had optimized the wall model using the vacuum magnetic field at MPA positions, the magnetic fields did not agree perfectly as shown in Fig. 5. The MPA signals also did not agree in the equilibrium analysis as shown in Fig. 9. In the original FCA method [8], the vacuum magnetic field is not obtained by the circuit equation but by the multipole expansion based on measurement of the vacuum field without plasma. The plasma shape and the position calculated by the FCA method using the circuit equation and the wall model used in this paper are compared with those calculated by the original FCA method. The results are shown in Fig. 14 for κ, R_{P} and a_{P} and in Fig. 15 for the cross-section of LCFS. From these figures, it was seen that κ is smaller and the horizontal radius of the plasma is larger in the original FCA than in the FCA using the circuit equation. Since the multipole method evaluates the vacuum magnetic field based on the experimental values of the magnetic field, it seems to be more reliable. The reason why we nevertheless used the FCA with the circuit equation is that it calculates the eddy current by solving the

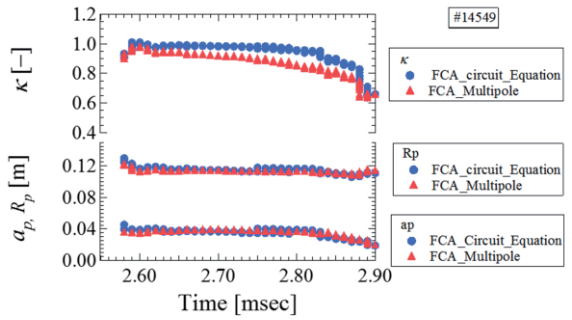

Fig. 14 The comparison of (top) the elongation and (bottom) the major and the minor radii calculated by the FCA using the circuit equation method (blue circles) and the multipole method (red triangles).

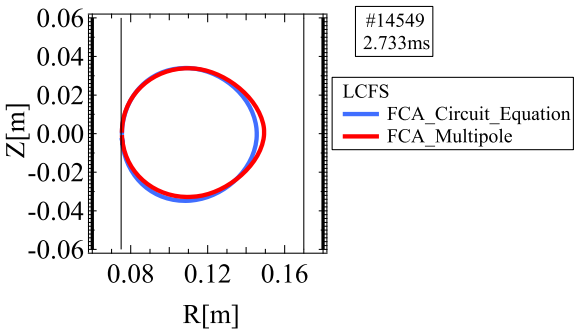

Fig. 15 The comparison of the last closed flux surface (LCFS) calculated by the FCA using the circuit equation method (blue) and the multipole method (red).

same equation with TOSCA and then we can compare the results of the eddy current calculated by FCA and TOSCA as the first step in establishment of the new equilibrium analysis method using TOSCA. In addition to the difference in the plasma shape, the values of β_P (= 0.36(sec4.2), 0.41(sec4.2)) are higher than we estimated ($\beta_P \sim 0.2$). This might also be due to the same cause. It is one of the future subjects to develop the way to reconstruct MHD equilibrium based on the results of FCA using the multipole method.

6. Summary and Future Plan

The equilibrium analysis including the eddy current effect was performed for TOKASTAR-2 tokamak plasma by using the TOSCA code. The eddy current was calculated using 2D axisymmetric models of the vacuum vessel. To consider the actual 3D structure of the TOKASTAR-2 vessel and installation errors of coils and magnetic sensors, we determined the optimal model using parameter scan. In the equilibrium analysis, the plasma boundary was fixed to that obtained by the filament current approximation method and the values of l_i and β_P were determined to have the free coil (PVF coil) current equal to the experimental value and minimize the errors between the calculated values and the experimental values of the external magnetic field.

For the first step to verify the equilibrium solution determined by the external measurements only, the magnetic field inside the plasma was measured by the magnetic probe inserted to the plasma. The difference in l_i in two equilibrium solutions with external and internal measurements was 0.10, or not so large. The equilibrium determination with external measurement seems to be promising at least for rough estimation of the current density profile, though we need to compare for many shots with various discharge conditions. We considered that the cause of difference was the wall model because the calculated magnetic field values at the magnetic probe array positions was not perfectly matched with the experimental measurement.

In the future, we will improve the wall model so that it can reproduce the experimental magnetic field and see if the equilibrium solution with the external measurement will be closer to the internal measurements and the high-speed came images. In addition, it is one of the future subjects to identify the reason why we can evaluate β_P and l_i separately for a circular plasma by using the external field measurement only.

Acknowledgments

This work is partly supported by the NIFS Joint Use Program of Measurement Instruments and Collaboration Research Program (NIFS17KLEP026).

[1] T. Oishi, K. Yamazaki, K. Okano *et al.*, J. Plasma Fusion Res. SERIES **9**, 69 (2010).
[2] M. Hasegawa, K. Yamazaki, H. Arimoto *et al.*, Plasma Fusion Res. **7**, 2402116 (2012).
[3] R. Nishimura, H. Arimoto, T. Fujita *et al.*, Plasma Fusion Res. **9**, 3402059 (2014).
[4] H. Ikezi, K.F. Schwarzenegger and C. Ludescher, Phys. Fluids **22**, 2009 (1979).
[5] T. Ueda, H. Arimoto, T. Fujita *et al.*, Plasma Fusion Res. **10**, 3402065 (2015).
[6] K. Muraoka, T. Fujita, H. Arimoto *et al.*, Plasma Fusion Res. **13**, 1402111 (2018).
[7] T. Sakito, H. Arimoto, T. Fujita *et al.*, Plasma Fusion Res. **11**, 2402074 (2016).
[8] K. Yasuda, H. Arimoto, T. Fujita *et al.*, Plasma Fusion Res. **13**, 3402072 (2018).
[9] D.W. Swain and G.H. Nilson, Nucl. Fusion **22**, 1015 (1982).
[10] L.L. Lao, H. St. John, R.D. Stambaugh *et al.*, Nucl. Fusion **25,** 1611 (1985).
[11] V.S. Mukhovatov and V.D. Shafranov, Nucl. Fusion **11**, 605 (1971).
[12] R. Yokoyama, A. Okamoto T. Fujita *et al.*, Plasma Fusion Res. **13**, 3402047 (2018).